Smart Energy and Sustainable Environment

2023, *26*(1): 13-28, https://doi.org/10.46390/j.smensuen.26123.453

DEUTERIUM RETENTION IN *N*-SEEDED AND UNSEEDED TUNGSTEN LAYERS OBTAINED WITH *DCMS* AND M-*HIPIMS* TECHNIQUE

Oana Gloria Pompilian[1], Paul Dinca[1], Ion Burducea[2], Flaviu Baiasu[1,3], Cornel Staicu[1,3*]

[1]*National Institute for Lasers, Plasma and Radiation Physics, Bucharest 077125, Romania*
[2]*Horia Hulubei National Institute of Physics and Nuclear Engineering, IFIN-HH, Magurele*
[3]*Doctoral School of Physics, University of Bucharest, Romania, 077125, Romania*

Abstract:

The retention of hydrogen isotopes in tungsten co-deposited layers is a subject severely understudied in the literature compared to hydrogen isotope implantation in bulk tungsten specimens. However, impurity seeding in future next-generation fusion devices can reduce the sputtering threshold of tungsten and potentially increase the contribution of the tungsten layers to the global tritium retention problem. This paper reports on the development of fusion-relevant tungsten-deuterium and nitrogen-seeded tungsten deuterium layers using direct current (DCMS) and multipulse high-power impulse magnetron sputtering techniques (HiPIMS). The four layers resulting from co-deposition in argon-deuterium and argon-deuterium-nitrogen atmosphere were investigated from the deuterium retention and release point of view. Supplementary the crystalline structure of all samples and particularly the composition of the nitrogen-seeded layers were also studied. The tungsten-deuterium layers produced using m-HiPIMS technology showed a higher crystalline coherence compared to layers deposited with DCMS in part owned to the enhanced ion bombardment of the forming layers during deposition. On the other hand, the nitrogen-seeded layers showed without exception the formation of the tungsten-nitride compound. Here on the contrary the crystalline coherence as revealed by X-ray diffraction measurements measurement showed that nitride formation is favored for DCMS compared with m-HiPIMS. The elemental areal densities of the layer constituents were analyzed using Rutherford Backscattering Spectrometry. In this case, only the two nitrogen-seeded layers were analyzed revealing that a higher nitrogen content by a factor of ~2 is retained in DCMS deposited layer compared to HiPIMS.The release of deuterium was higher in the case of m-HiPIMS layers and it was shown that despite the deposition method the release behavior occurs predominantly at temperatures above 800 K suggesting a high energy trapping of deuterium in tungsten layers. Nitrogen seeding influences both the retention mechanisms and increases the deuterium retention by two orders of magnitude in seeded layers compared to unseeded ones.

Article info:

Received 28 April 2023
Received in revised form 15 May 2023
Accepted 06 June 2023
Available online 09 June 2023

Keywords*:*
Tungsten, Hydrogen isotopes, DC, HiPIMS, Thermal Desorption Spectroscopy

[*]*Corresponding author: Cornel Staicu, e-mail: cornel.staicu@inflpr.ro*

The influence of How to cite: Pompilian O. G., Dinca P., Burducea I., Baiasu F., Staicu C., (2023). Deuterium retention in N-seeded and unseeded tungsten layers obtained with DCMS and m-HiPIMS technique. *Smart Energy and Sustainable Environment*, *26*(1), 13-28, 2023, https://doi.org/10.46390/j.smensuen.26123.453.

1. INTRODUCTION

One of the key elements required for the emergence and growth of civilization is energy. The high development and comfort standards encountered today in the Western world and in highly industrialized countries translate also into high energy consumption. At the same time increasing the living standards in poor countries and the growing energy demands in developing countries puts a high strain on the already dwindling resources required to produce energy. The accelerated development of human civilization in the last 200 years, triggered at first by the industrial revolutions, has at its core the availability of cheap energy which was obtained then and now by burning fossil fuels. Fast-forward to today in the 21st fossil fuels are still primarily used to cover the energy requirements of our civilization. However, this addiction to this cheap resource also generates grave global consequences, and it is necessary to act fast to mitigate these unwanted effects. Problems like water-source and in general environmental pollution, degrading air quality especially in crowded cities due mainly to transportation and industry, and large greenhouse emissions which trigger catastrophic climate changes; make stringent the transition to renewable and clean energy sources (United Nations Development Programme Human Development Report 2016; Rubel M. et all, 2011). Many of the main candidate's sources of energy like solar and wind are plagued by discontinuity in production (day-night cycle, less windy days) requiring expensive storage systems in order to ensure continuous delivery to consumers. Despite historical setbacks and the long development time nuclear fusion is still representing one of humanity's best chances for durable development in the future. Among the many traits that make it attractive, we can enumerate virtually unlimited fuel abundance, no environmental pollution, large quantities of energy, and continuous production.

Currently, it consists in fusing light hydrogen isotopes, deuterium (D) and tritium (T), in a tokamak-type device. Among the many experimental fusion devices, the one currently build, in Kadarache, France, namely the International Thermonuclear Experimental Device (ITER), will be responsible to make the transition of nuclear fusion from experiment to production. Among the many problems that plagued the technology during the design and engineering phase of the ITER tokamak, plasma–wall interaction represents an important one that needs to be solved in order to make accurate predictions and demonstrate the viability of the fusion technology.

The interaction of the fusion plasma with the inner physical boundaries of the tokamak is responsible for the erosion, melting, and co-deposition of the materials that enter into the composition of the plasma-facing components (PFC). Plasma-induced material migration in the tokamak inner vessel presents multiple problems for the normal functioning of the fusion reactor. Firstly material migration in plasma can result in a yield loss due to multiple excitation levels compared to hydrogen isotopes and afterward, the materials are re-deposited in thin layers on top of the PFC's changing inner vessel surface properties (Widdowson A. et all, 2019; Mayer M. et all, 2017). The co-deposited layers also retain nuclear fuel at higher levels compared with the walls.

This represents a big safety problem due to the volatile and radioactive properties of T, which on top of that is one of the scarcest gas is intended to be produced in situ through nuclear reactions (Zheng S. et all, 2016). From a safety and component point of view, ITER license as a nuclear facility allows no more than 1kg of mobilizable tritium to be retained, namely 300 g in the vacuum system ducts and 700 g of tritium in the inner vessel walls during its entire lifetime (Roth J., et all, 2008; Taylor N. et all, 2013).

Implantation of nuclear fuel in PFCs and co-deposition of the materials together with nuclear fuel will be the main drivers for inner wall T retention. The very high retention rate of nuclear fuel in carbon-based deposits in previous fusion devices (Krat S. et all, 2015) was one of

the most important reasons that this material will not enter the composition of the PFCs for ITER. For ITER the PFC design includes Be to cover the inner wall due to its plasma-compatible properties and in the hottest areas (divertor) W will be employed due to its sputtering resilience and refractory properties (Federici, G. et all, 2003; Federici, G. et all, 1999). As in previous C-based fusion devices, it is still expected in ITER that the main tritium accumulation channel will still be retention in co-deposited layers However, it is expected that the largest amounts of tritium will be retained primarily in Be co-deposited layers due to the low sputtering threshold for hydrogen isotopes (United Nations Development Programme Human Development Report 2016; Carpentier, S. et all, 2011; Schmid, K. et all, 2015). Even though these materials were selected to reduce fuel retention significant accumulation was observed in W (De Temmerman G., Doerner R.P. 2009; Alimov V.K. et all, 2010) and very high levels comparable with hydrocarbon layers in Be (Krat, S. et all, 2017; De Temmerman G. et all, 2008; Mayer M. et all, 1996). Unlike implantation studies (Zibrov M. et all, 2016; Johnson D.F., Carter E.A., 2010; Heinola, K. et all, 2010), retention in W co-deposited was largely neglected in literature and was addressed in a small number of studies (De Temmerman G., Doerner R.P. 2009; Wang P. et all, 2009; Krat S. et all, 2018; Qiao L. et all, 2018) because it was considered that retention in W is largely negligible considering the high sputtering threshold. As studies show impurity seeding is required for the cooling of the edge plasma in order to protect the structural integrity of the diverter and to mitigate the recurrence of high–power transient plasma events (Pacher G. W. et all, 2007; Kallenbach A. et all, 2011; Bisai N. et all, 2019). Primarily noble gases were considered potential candidates for seeding during the device's operation and however, they will surely affect the sputtering threshold of tungsten and potentially increase the formation rate of W layers. Amongst the gases employed for this purpose nitrogen (N) showed some promising results in tests performed in experimental fusion devices (Kallenbach A. et all, 2010). However, the presence of N in a fusion reactor like ITER can further complicate the retention of nuclear fuel in W-co-deposited layers due to problems related to nitride formation (Dinca P. et all, 2017).

In this paper, we present some experimental results concerning the deposition of tungsten-deuterium layers using direct current magnetron sputtering and high-power impulse magnetron sputtering. To ascertain the degree to which N influences the properties of the resulting layers N_2 gas was seeded in the reaction chamber for a couple of deposition batches and these samples were used for comparison with the tungsten-deuterium layers. Even though the study was focused on understanding the retention/release mechanisms of D from these layers, structural and compositional properties were also investigated.

2. MATERIALS AND METHODS

2.1. Layers Deposition

Tungsten layers with deuterium and nitrogen gas inclusion were prepared through co-deposition in reactive Ar-D atmosphere and Ar-D-N respectively. For comparison in terms of layer properties and deuterium retention and release behavior, two separate magnetron sputtering regimes were used. The first one consisted of the classical continuous current magnetron sputtering deposition (DCMS) and the second was the relatively novel multipulse-High Power Impulse Magnetron Sputtering generically known as m-HIPIMS.

In total four types of W coatings were prepared using the above methods. Layer deposition took place in a circular chamber with a diameter of 60 cm. Prior to deposition, ultrahigh vacuum conditions were attained using a turbomolecular pump (10^{-6} mbar) in order to reduce at the maximum possible level the residual gas contamination in the resulting coatings. The experimental design of the coating system is presented elsewhere in previous studies (Dinca P. et all, 2017; Dinca P. et all, 2021, Dinca P. et all, 2022) Silicon and graphite wafers with a size of 12x15 mm were used as substrates for the deposition. Before starting the deposition process, the substrates were ultrasonically cleaned in a solution of a mixture of acetone and isopropyl alcohol to remove impurities. The cleaning process lasted

15 minutes at a frequency of 45 kHz, after which the samples were washed abundantly with distilled water and were left to dry. The cleaned substrates were positioned on a solid support in front of the sputtering source at a fixed distance of 10 cm.

The deposition equipment presented below is composed of two water-cooled magnetrons provided with 2 mm thick and 50 mm in diameter ITER-grade purity tungsten targets (99.95%) The magnetron system consisted of two water-cooled cathodes equipped with two circular W targets (2 mm thick and 50 mm in diameter) of high purity (99.95%). One of the cathodes was operated in m-HiPIMS mode powered by a high-power pulse generator which in turn was triggered by a signal generator. The I-V characteristics and the shape of the pulses were recorded using an oscilloscope. The other W cathode was operated in DC mode using a current-limited high-voltage power supply. After the base pressure of 10^{-6} mbar was reached 20 ml/min of high-purity argon (Ar) gas was introduced in the reaction chamber via a calibrated mass flow controller. This, in turn, raised the pressure up to 10^{-2} mbar. The Ar gas was used to ignite a glow discharge by biasing the substrates (-200 V) with the purpose of removing surface impurities. Finally by placing an obturator in between the sputtering source and the deposition substrates the W targets were cleaned in DC-mode to also remove impurities and to ensure good bonding between the deposited layer and the substrate which was essential considering the low roughness of the Si wafers (5 nm) and the C rectangular substrates (mean roughness of 50 nm).

Table 1. Deposition parameters of the W+D and W+D+N layers in HiPIMS and DCMS mode

Proba	***W HiPIMS***					***W DCMS***		
	Frequency (Hz)	**Voltage (V)**	**Current (A)**	**Pulse width (µs)**	**Deposition rate (Å /s)**	**Voltage (V)**	**Current (mA)**	**Deposition rate (Å /s)**
W+D	1000	900	10	5	0.90	390	150	0.90
W+D+N	1000	900	15	5	0.90	350	150	0.90

As it was said early depositions were performed in a reactive sputtering regime. In the first case (Ar-D), D was introduced gradually after the target cleaning while maintaining the discharge ignited. The final Ar-D gas mixture ratio was 1:1 and consisted of a 30 ml/min flow rate for each gas. In the second case (Ar-D-N), both D and N were introduced simultaneously, however in this case the ratio was 1:2:1, raising the D flow rate to 60 ml/min. Even though the quantitative differences between the nuclear fuel and impurities in the ITER edge plasma are significantly higher, in this case, we only doubled the D flow rate compared to nitrogen (from 30 ml/ min in the previous case to 60 ml/min). During all performed coatings the pressure inside the reaction chamber was kept constant at $2*10^{-2}$ mbar which was achieved by adjusting the rotational speed of the turbo-molecular pump

The W deposition parameters for both m-HiPIMS and DCMS mode are presented in Table 1. It can be observed in HiPIMS mode that both repetition frequency and pulse width in HiPIMS mode were the same for both deposited layers. While the repetition frequency influences the deposition rate, pulse width influences mainly the ionization degree of the plasma as well as the ion composition. A low pulse duration ensures a gas ion-dominated plasma while at higher pulse duration plasma is dominated by metallic ions. As it was demonstrated in a previous study the gas implantation process is enhanced at low pulse durations. In DC mode we can see that the addition of nitrogen is leading to a voltage drop while in m-HiPIMS mode the current increases. This can be correlated with the tungsten target poisoning, thus by introducing N in the mixture WN-nitride-type compound is formed at the target surface which enhances the secondary electron emission and increases the ionization degree. Also, it is obvious that the difference between the two sputtering modes is represented by the ionization degree which is massive in m-HiPIMS

mode compared to DCMS. Deposition rate was measured prior to each coating process by positioning a quartz micro-balance in front of the sputtering source in the virtual position of the substrates. Since this is an important parameter that can influence the D retention properties (De Temmerman G. et all, 2008) it was maintained at a constant value of 0.9 Å/s for all deposited layers.

2.2. Investigation Methods

2.2.1. XRD Investigations

The crystalline structure of the investigated W-D and W-D-N type layers was assessed using the X-Ray Diffraction method (XRD). For this purpose, a Bruker D8 Advanced diffractometer was used. The equipment is provided with a Cu-Kα X-Ray source type with a specific wavelength of XRD was the choice method to peer into the crystalline nature of the deposited samples 1.54 Å. For the measurements, a classical Bragg-Bretano geometry was employed. Considering the polycrystalline nature of the deposited W layers and in order to avoid the overlapping of the peaks corresponding to the substrate with the ones generated by the deposited layers, only layers deposited on monocrystalline silicon substrates (hkl = [111]) were investigated. During measurements, a large sweep range between 20^o and 110^o was used to identify as many hkl orientations as possible. Furthermore, for good counting statistics, a small step of 0.01^o with a large integration time per step (4 s) was used.

2.2.2. RBS Analysis

To obtain information concerning the chemical composition of the deposited layers the samples were analyzed using Rutherford backscattering spectrometry (RBS). The result will not include the investigations performed on W-D layers due to the fact that with RBS we cannot quantify the level of D in the samples and we focused only on measuring the N in depth concentrations in W-D-N samples. The results are important since N can heavily influence the D retention/release due to its chemical reactiveness with tungsten witch as was shown above from the XRD measurements leads to the formation of nitride compounds. The ion beam analysis measurements were carried out using the 3 MV Tandem Accelerator facility from IFIN-HH (Burducea I. et all, 2015). For a better quantification of the elements, the only analyzed samples were deposited of graphite substrates since it avoids overlapping the substrate signal with the one generated by the presence of N in the layer. For the actual measurements samples were mounted on a high precision (0.01^o) goniometric holder in a vacuum chamber. Prior to the measurements, the chamber was pumped down to a base pressure of 10^{-5} Pa after which the samples were exposed 2.6 MeV monoenergetic $^4He^+$ ion beam at normal incidence. A solid-state detector positioned at an incidence angle of 165^o in relation to the ion beam was used to measure the energy of the backscattered particles. A Faraday Cup detector was employed to measure the accumulated charge. The final value for each sample was 10 μC ensuring that both samples were exposed to a similar number of charged particles for a good statistic. To identify and quantify the layer constituent elements the experimental spectra were fitted using the SIMRA software developed at IPP Garching (Mayer M., 1997)

2.2.3. TDS Analysis

The release of D from W-D and W-N-D layers was investigated using Thermal Desorption spectroscopy. For this purpose, only the layers deposited on Si substrate were analysed due to the destructive nature of the technique. The measured samples were heated up to a final temperature of 1325 K using a heating rate of 10 K/min. Deuterium was quantified based

on molecular deuterium (D_2, mass 4) and deuterium hydride signal (HD, mass 3), monitored during the heating process by a quadrupole mass spectrometer. The experimental setup employed for the measurement is illustrated and described elsewhere (Dinca P. et all. 2017). To accurately transform the ion current signal in molecular flow calibrations were performed prior to the actual measurements. During calibrations, a small flow of interest gas is introduced in a similar geometry as in the actual measurements. The molecular flow is controlled by a mass flow controller (calibrated for the input gas) which was connected in line with the quadrupole mass spectrometer. To obtain a good statistic for the D_2 calibration factor five D_2 flows were introduced at a constant rate between 0.01-0.05 s.c.c.m, each flow was on for 60 s while the resulting current was measured by the quadrupole spectrometer until background levels were restored. The D_2 resulting calibration factor was calculated as the mean average of the values obtained for different D_2 flows. For HD instead, H_2 gas was employed using the same procedure and flows as in the case of D_2. In this case the HD calibration factor was calculated as the mean average between D_2 and HD factor. The D desorption curves below were obtained by summing the contributions of the HD integrated signal with the D_2 signal. Furthermore, the desorption was normalized to the surface area (cm^2).

2.3. Results

2.3.1. Crystalline Structure

The X-ray diffractograms presented above in figure 1 show a comparison between the W layers deposited in HiPIMS and DCMS mode in Ar-D reactive atmosphere. From the diffraction patterns, we identified several peaks corresponding to a metallic W room temperature phase crystalline phase, Im-3m space group, with the atoms of the unit cell arranged in a volume-centered cubic structure. From the X-ray diffractograms obtained for the samples synthesized in both DC and HiPIMS modes, the corresponding orientations W(110), W(200), W(211), W(220), and W(310) were identified based on the JPSD cards. As it can be clearly seen in Figure 1 the W(110) represents the dominant peak from the diffraction pattern meaning that the crystallites have preferential growth on this plane for both deposition techniques This preferred crystalline growth as well as the relationship between the intensities of the diffraction maxima, resemble the reference crystalline growth of W.

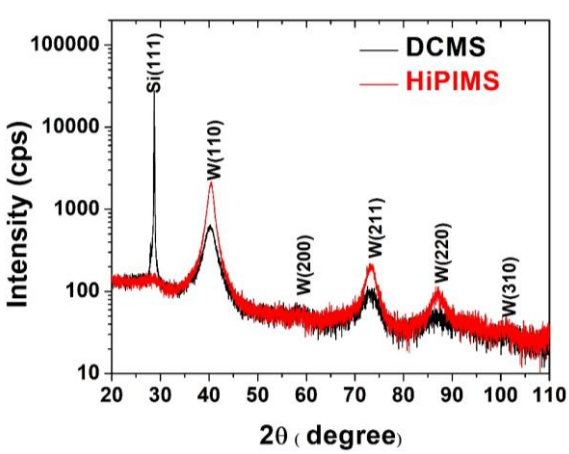

Figure 1. X-ray diffraction pattern of W-D layers deposited in DCMS /HiPIMS mode

The main crystalline structure differences between the layers presented in figure 1 can also be primarily noticed from the intensity ratio between the diffraction peaks. There can be noted an increase of 300%, 250% and 200% for W110, W211, and W310 orientations for the HiPIMS deposited W layer in comparison with DCMS. These findings might suggest that the higher ionization yield obtained in HiPIMS mode compared to DCMS can also be translated to an increase of the ion bombardment on the growing layers during deposition, which improves the ad-atom mobility and diffusion which enhances the crystalline structure. This is particulary evidenced by the results obtained from the peak analysis which are presented in table one. They show both an increase in crystalline coherence length from 4.4 nm to 6.9 nm as well as an increase in the crystalline degree from 66.2% to 70.2%, for HiPIMS compared to DCMS deposited layers. Furthermore, besides the sharp Si (111) peak corresponding to the substrate, there can be observed a broad appearance of the W crystalline phase corresponding peaks. This feature might indicate a systemic micro-stress induced in the crystalline lattice most likely by the presence of the gas inclusions in the layer.

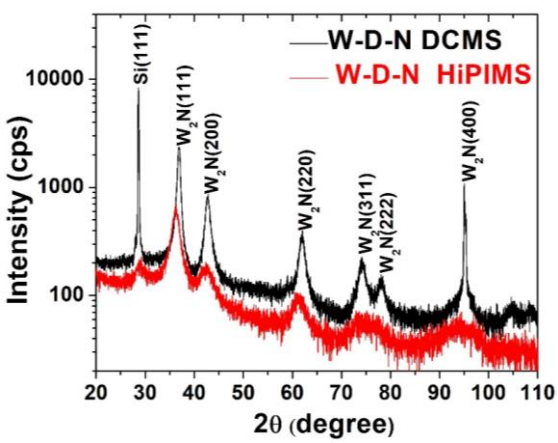

Figure 2. X-ray diffraction pattern of W-D layers deposited in DCMS /HiPIMS mode

The diffraction patterns of the W layers deposited in the Ar-D-N reactive atmosphere in HiPIMS and DCMS mode are illustrated above in Figure 2. The following diffraction peaks corresponding to hkl orientations were identified: W_2N 111, W_2N 200, W_2N 220, W_2N 311, W_2N 222 and W_2N 400. These peaks correspond to a tungsten nitride W_2N tf crystalline phase, Fm-3m phase. This crystalline compound is formed for both techniques employed in W-layer deposition. Table 2 presents the main cristalline structure parameters derived from the analysis of the diffraction peaks observed in Figure 1 and Figure 2. The cristalline coherence length (D_{eff}) commonly reffered as the crystallite grain size was calculate by fitting the W 110 and WN 111 with a Voigt function from which a beta Lorentz factor was extrapolated and introduced in the below formula:

$$D_{eff} = \frac{K*\lambda}{\beta_L*\cos(2\theta)} \quad (1)$$

where, K is a constant equal to 0.9, λ is the specific wavelength of the X-ray radiation (0.154 nm), β_L is the beta Lorentz factor obtained from the fitting of the diffraction peak with a Voigt function and 2θ is the diffraction angle.

Besides the crystalline coherence length the amorphization and the crystalline degree are also presented in table 1. The amorphization degrees was calculated with:

$$Amorphization\ degree = \frac{Diffraction\ pattern\ area - Crystalline\ peak\ area}{Diffraction\ pattern\ area} * 100 \quad (2)$$

while the crystalline degree is:

$$Crystalline\ degree = 100 - Amorphization\ degree$$

Moreover, in contrast with the diffraction patterns of W deposited in the Ar-D atmosphere here, we can observe a much more coherent crystalline growth for the W+D+N samples deposited in DCMS compared to the HiPIMS mode. This is somewhat of a counter-intuitive behavior since it is expected that the addition of nitrogen should increase the ion bombardment of the growing layers in HiPIMS mode, thus enhancing the crystalline structure. On the opposite, the addition of nitrogen here seems to lead to a refinement of the crystallites (smaller grain size) and a significant layer amorphization as it is clearly evidenced by the results presented in table 2.

Table 2. Crystalline structure parameters derived from the peak analysis of the corresponding diffraction patterns

Sample	***D_{eff}* (nm)**	***Amorphization Degree* (%)**	***Crystalline Degree* (%)**	***Lattice constant* (Å)**
W+D DCMS	6.9	33.8	66.2	2.24
W+D HiPIMS	4.4	29.8	70.2	2.23
W+D+N DCMS	13.8	27.5	72.5	2.44
W+D+N HiPIMS	6.8	36.1	63.9	2.48

At a closer look at the diffraction pattern, one might observe a shifting of the W_2N peaks towards a lower angle for layers deposited in HiPIMS compared to DCMS, which can potentially give an explanation for the strange behavior observed in Figure 2. This shift indicates the presence of a nonuniform compressive stress which enlarges the lattice spacing slightly reducing the diffraction angles. As was demonstrated in a previous work HiPIMS operated a lower pulse width enhances the retention of gas ions in the layers. Thus, it is expected that besides chemical bonding with W nitrogen is also retained interstitially straining the W lattice and reducing the crystalline coherence of the layers as it is evidenced in table 2 where a reduction by a factor of 2 was observed in HiPIMS compared to DC. This effect is of course more pronounced for layers deposited in HiPIMS due to more intense bombardment with N ions.

2.3.2. Layer Composition

The experimental RBS spectra for W-D-N layers deposited with DCMS technology and HiPIMS technology, respectively are presented in Figure 3. The red line represents the simulated spectra plotted on top of the experimental result. The areal densities were extrapolated for the main layer constituents namely W, N, and graphite as well as the O impurity content. The energy loss of the particles in a given material is influenced both by the chemical nature of the material and the layer thickness, respectively

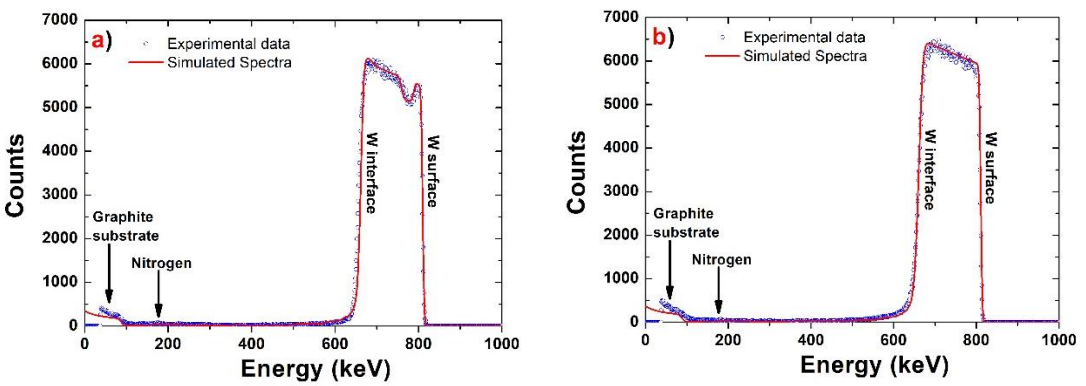

Figure 3. Experimental RBS spectra resulted from the analysis of W-D-N layers deposited using a) direct current magnetron sputtering technology and b) high-power impulse magnetron sputtering. The red line represents the fitting of the experimental data using SIMRA computer code.

The experimental RBS spectra for W-D-N layers deposited with DCMS technology and HiPIMS technology, respectively are presented in Figure 3. The red line represents the simulated spectra plotted on top of the experimental result. The areal densities were extrapolated for the main layer constituents namely W, N, and graphite as well as the O impurity content. The energy loss of the particles in a given material is influenced both by the chemical nature of the material and the layer thickness, respectively. Here the Y axis provides information regarding the relative elemental abundance in the layers while de X axis allows for the identification of the elements. It can be seen from Figure 3 that there is a very good correlation between the experimental data and the simulated SIMRA spectra for each layer, which in turn will translate into precise identification of the elemental areal densities. It can be clearly noticed that the highest peak in Figure 3 is represented by the W layer. In both cases the typical signal presents a sharp rise, this signal is given by the interaction of the He ions with the W layer surface. The interaction of the He ions with the interface region between the W and the graphite substrate is characterized by a fast decrease in the W signal. Compared to the surface in this case the signal's edge resembles an elongated tail. This elongation becomes more pronounced for higher substrate roughness affecting the simulation precision.

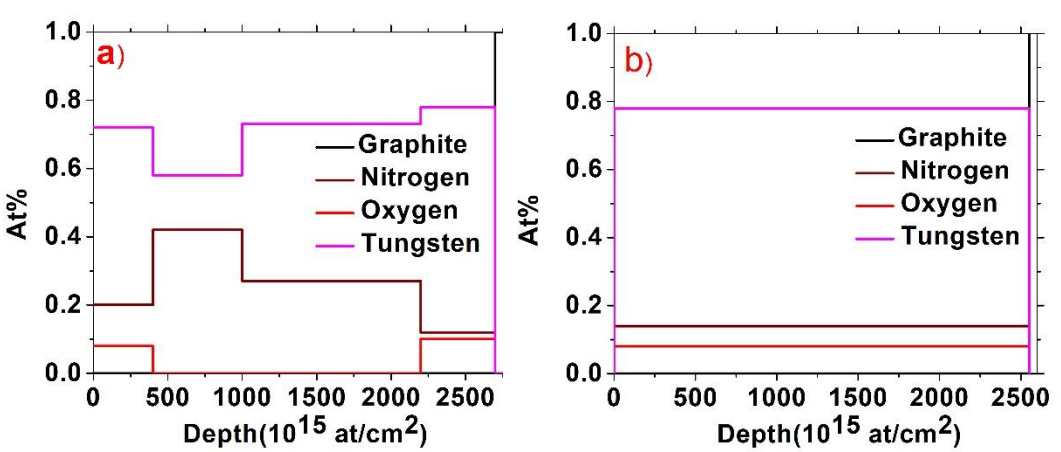

Figure 4. Elemental depth profile illustrating the in-depth concentration of elements in W-D-N layers deposited in a) DCMS mode and b) HiPIMS respectively.

The depth profile of the elements in W-D-N layers deposited in DCMS and HiPIMS mode, resulting from the simulation of their corresponding experimental RBS spectra with SIMRA, are presented above in Figure 4. The sample stoichiometry was evaluated based on the determined areal densities of the layers. In the case of the W-D-N sample deposited in HiPIMS regime, the areal densities were the following: 1990 ± 100 x 10^{15} at/cm^2 for W, 360 ± 18 x 10^{15} at/cm^2 for N, and 200 ± 10 x 10^{15} at/cm^2 for O which correspond to a sample mean atomic composition of $W_{0.78}N_{0.14}O_{0.08}$. Here (Fig 5b), it can be noticed that both W and N, as well as the O impurity, have uniform elemental distribution in layer depth. In comparison, the layer obtained with DCMS (Figure 4a) presents a non-uniform distribution of the elements. The surface and the substrate layer interface proved considerably difficult to simulate, in terms of elemental mixing requiring a higher number of layers. Unlike Figure 4b) the O contamination is only limited to the surface and the interface region possibly related to contamination from air exposure as well as from the diffusion of O from the substrate into the layer. For the DCMS deposited layer based on the determined areal densities of 1900 ± 95 x 10^{15} at/cm^2 for W, 640 ± 32 x 10^{15} at/cm^2 for N, and 150 ± 8 x 10^{15} at/cm^2 for O; the atomic composition of the layer was $W_{0.70}N_{0.24}O_{0.06}$. A comparison between the two samples presented above clearly shows that the N content in W-D-N layers deposited in DCMS mode is almost double compared to the one obtained through HiPIMS. Thus, it can be concluded that in DCMS additional trapping sites for N are created or that nitride formation is enhanced as it was shown above from the XRD measurements.

The thickness of the deposited layers can be evaluated based on the areal density of tungsten. To make the conversion from areal density to nm we assumed a reference bulk density of 19.29 g/cm^3 and a uniform distribution of W atoms. The results point to a lower thickness than expected of 315 nm for the HiPIMS deposited layers and 300 nm for DCMS. However, the differences between the assumed bulk density and the layer density can be significantly larger considering nitride formation and thus the conversion might be prone to errors. (Malinský, P. et all, 2012)

2.3.3. Deuterium Desorption

The experimental TDS spectra concerning the D release kinematics from W layers deposited in D and D-N reactive atmosphere with the DCMS method and m-HiPIMS respectively are presented above in Figure 5. The experimental spectra of D release from the W-D layer deposited in DCMS are illustrated in the upper left corner of Figure 5a). Here, the D desorption has an onset at 400 K and has a sharp rise up to 500 K after which a constant desorption is observed in the 500 -600 K temperature range. It can be noticed from the desorption continues to rise with temperature even above 700 K. As it can be observed compared to the rest of the desorption curves presented in Figure 5 the desorption for the W-D sample deposited with DCMS suddenly stops at 750 K. During the measurements most likely due to a number of factors among them: the lattice mismatch between the Si substrate and W layer, the poor adhesion due mainly neutral nucleation, low ion bombardment of substrate-layer interface and different thermal expansion coefficients; the W layer delaminated from the Si layer. Sudden delamination of the layers is usually accompanied by a fast and large increase of the D signal. However, in this case due to the abrupt shift in pressure, the QMS entered in protection mode not recording the corresponding deuterium release. So, in the following a quantitative analysis of the deuterium released from this sample is not possible.

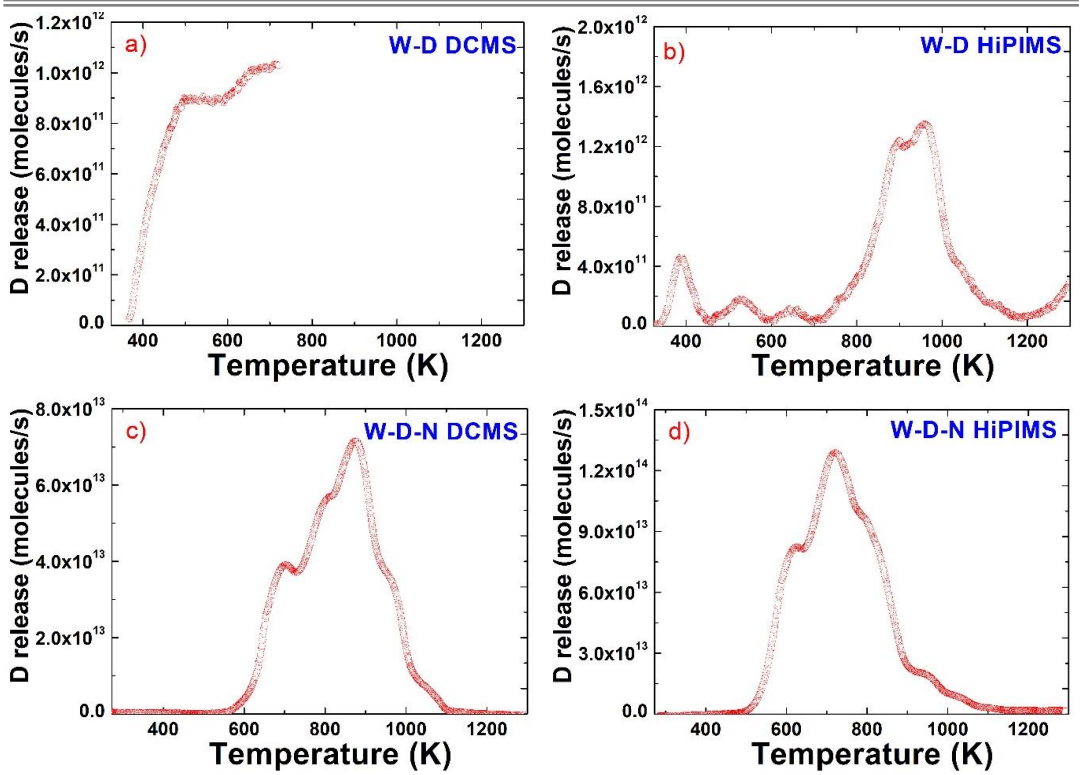

Figure 5. Experimental desorption curves of deuterium from Unseeded and N-seeded tungsten co-deposited layers

The experimental TDS spectra concerning the D release kinematics from W layers deposited in D and D-N reactive atmosphere with the DCMS method and m-HiPIMS respectively are presented above in Figure 5. The experimental spectra of D release from the W-D layer deposited in DCMS are illustrated in the upper left corner of Figure 5a. Here, the D desorption has an onset at 400K and has a sharp rise up to 500K after which a constant desorption is observed in the 500-600K temperature range. It can be noticed from the desorption continues to rise with temperature even above 700K. As it can be observed compared to the rest of the desorption curves presented in Figure 5 the desorption for the W-D sample deposited with DCMS suddenly stops at 750K. During the measurements most likely due to a number of factors among them: the lattice mismatch between the Si substrate and W layer, the poor adhesion due mainly neutral nucleation, low ion bombardment of substrate-layer interface and different thermal expansion coefficients; the W layer delaminated from the Si layer. Sudden delamination of the layers is usually accompanied by a fast and large increase of the D signal. However, in this case due to the abrupt shift in pressure, the QMS entered in protection mode not recording the corresponding deuterium release. So, in the following a quantitative analysis of the deuterium released from this sample is not possible.

The desorption chart of the W-D layer deposited in m-HiPIMS mode is presented in Figure 5b. The release behaviour presented here might evidence a multiple trapping retention of D in tungsten layers. Considering the limited data available we can at least make a comparison with the TDS chart presented in Figure 5a for W-D deposited in DCMS up to a temperature of 750K. Here also the desorption onsets at a very low temperature of 340K suggesting that both samples present a strong low energy release

component which is higher compared to studies performed through implantation. This behaviour might be determined by the higher D fluence of the samples compared to a previous study. A difference compared to the sample deposited in DCMS is related to the first desorption feature which here (Figure 5b) is clearly defined between 340-450K with a relatively sharp peak at 390K. This peculiar release is seldom encountered in literature and can be possibly attributed to a surface retention of deuterium in interstitial trapping sites which might explain the low release temperature. This desorption feature is lately followed by a broad release in the temperature range 450-600K with a maximum intensity at ~530K. This type of release was observed in other studies performed with co-deposited W layers performed by Wang (Wang, P. et all, 2014; Wang, P. et all, 2015) and Poon (Poon M. et all, 2008). In their works they observed a peak release of deuterium at 520K. However, there is a divergence between the studies concerning the mechanism of retention in this particular trap. On one hand, Wang considers that the release observed at 520K is attributed to D trapping in intrinsic layer defects such as grain boundaries and dislocations. However, this type of explanation is very general and it was used in multiple studies mainly to explain the D retention in implanted bulk tungsten. On the other hand, in his modelling work of D trapping in W Poons implies that the 520K peak can be attributed to the de-trapping of both molecular and atomic D from vacancies. This explanation seems more plausible for our study considering that this type of defect can be created during layer growth from the intense bombardment generated by the plasma source. In between the 600-700K range a „shoulder type" small release can be observed with a not-so-obvious peak at 650K. The release can also be attributed to the de-trapping of D from vacancies, in this case with higher bonding energy. The largest part of the D inventory retained in the sample is released through a main broad desorption feature in 700-1150K range which presents two distinctive peaks at 900K and 960K. This release behaviour suggests a high energy trapping of D into the W layer. By integrating the contribution of different retention mechanisms, we can observe that the majority of the D ~85% is released at a temperature in excess of 800K and only a small inventory is released below this temperature. High energy trapping in W was also explained by Poons suggesting that D in this case is retained on the inner surface of voids present in the layer. The voids originate from the clustering of vacancies as explained in Poons work. In a previous work performed by the authors on mixed Be-W layers deposited by DCMS there is also a desorption chart for a W reference layer with a thickness of 500nm deposited with DCMS in Ar-D atmosphere (Dinca, P. et all, 2022). Even though the deposition parameters are not similar, and thus a quantitative comparison is impossible, the trapping behaviour can be compared to evaluate differences between the m- HiPIMS and DCMS methods. It can be seen that with DCMS the D is mainly released at low temperatures compared to m-HiPIMS, with the largest part of the D inventory being released at temperatures below 700K. From the limited results we have now it can be concluded that for W layers deposited with DCMS technique the largest part of the D inventory is trapped in the molecular and atomic form in vacancies with various binding energies and that the samples resulted from m-HiPIMS deposition exhibit a high energy trapping of D which might suggest according to literature that void-like type defects are created in these layers during deposition.

Figure 5c and 5d illustrate the deuterium desorption charts from W deposited in D and N reactive atmosphere with DCMS (Figure 5c) and m-HiPIMS techniques (Figure 5d). Both desorption charts present a large desorption feature that can encompass multiple trapping mechanisms however significant differences in terms of release temperature can be observed and they will be discussed below. The DCMS deposited layer shows an onset

of desorption at temperatures above 550K with a peak desorption at 876K. Also, several desorption features can be observed at 700K, 970K, and 1070K, on top of the main release chart which can point out to different trapping mechanisms. From the analysis of the desorption chart, it was established here that two-thirds of the deuterium inventory is released at temperatures between 800-1000K while only a third is released at temperatures below 800K. Compared to a previous study (Dinca, P. et all, 2022) where only a third is retained in high energy traps here, we can conclude that the addition of nitrogen during the deposition shifts the trapping behaviour of D towards higher temperatures. The same conclusion was also reached in a previous study performed by the authors where D retention was investigated in mixed Be-W layers seeded/unseeded during deposition with nitrogen. It was shown that N influences the D desorption temperatures shifting the release peaks with 100 K. As well as in the case of DCMS deposited layer, the m-HiPIMS (Figure 5d) desorption chart point to multiple features observed at 630K, 810K, 953K, and 1040K besides the main release peak at 720K. However, the similarities end here, we can observe that the peak release is 120K lower compared to Figure 5c and also has a higher intensity suggesting an enhanced D trapping in layers deposited with HiPIMS method. In terms of D release, we can notice that it occurs at lower temperatures for N-seeded layers (Figure 5 d)) compared to unseeded ones (Figure 5b). For W-D samples more than 80% of the total D inventory is released at a temperature above 800K while on the other hand, only 25% of inventory is released for the W-D-N layer with the rest of 75% being released in 600 K-800K temperature range.

The most important difference between the N seeded and the unseeded layers concerns the D inventory. It is noticeable from the desorption curves presented in Figure 5 that the quantity of D released from the sample is increased by almost two orders of magnitude compared to N-seeded samples. The results lead to the conclusion that nitrogen can affect the trapping mechanisms in W and thus influence the deuterium retention/release behaviour as well as increase the D inventory in the W layers. Both effects produced by N seeding can potentially be highly detrimental to the normal operation of a fusion reactor if N will be used as a seeding gas in conjecture with W plasma-facing components.

4. CONCLUSIONS

DCMS and m-HiPIMS techniques were successfully employed for the production of fusion-relevant W-D layers and also N seeded W-D layers. The crystalline structure of the layers is highly dependent on the deposition technique. W-D layers deposited in HiPIMS mode exhibited a better crystalline coherence in comparison to DCMS deposited samples. On the other hand, nitride formation is enhanced in DCMS mode. Layer composition shows that despite higher ion bombardment in HiPIMS mode N retention is lower compared to DCMS by a factor of ~2. D release from the samples showed that samples deposited in HiPIMS mode exhibited a higher D retention. The N seeding during deposition increases the D inventory in layers and influences retention properties.

Acknowledgement: This research was supported (or financed) by Romanian Ministry of Research, Innovation and Digitalization under Romanian National Core Program LAPLAS VII – contract no. 30N/2023.

Author contributions: Conceptualization: O.P., P.D.; methodology: C.S., validation: P.D., investigation: F.B., C.S., I.B., O.P.; data curation: P.D., O.P.; writing-original draft preparation: O.P., P.D.; writing-review and editing: P.D., C.S..; Visualization: C.S.; Supervision: P.D., and Project administration: O.P., C. S. All authors have read and agreed to the published version of the manuscript.

Conflict of Interest Statement: The authors declare no conflict of interest.

REFERENCES

Alimov, V.K.; Roth, J.; Shu, W.M.; Komarov, D.A.; Isobe, K.; Yamanishi, T.; (2010) Deuterium trapping in tungsten deposition layers formed by deuterium plasma sputtering. *J. Nucl. Mater.; 399* doi: 10.1016/j.jnucmat.2010.01.024.

Bisai, N.; Chowdhuri, M.B.; Banerjee, S.; Raj, H.; Dey, R.; Tanna, R.L.; Manchanda, R.; Jadeja, K.A.; Ghosh, J. (2019) Dynamics of neon ions after neon gas seeding into tokamak plasma, *Nuclear Fusion, 59,* doi:10.1088/1741-4326/ab3d31.

Burducea, I.; Straticiuc, M.; Ghiţa, D.G.; Moşu, D. V.; Cəlinescu, C.I.; Podaru, N.C.; Mous, D.J.W.; Ursu, I.; Zamfir, N. V. (2015) A new ion beam facility based on a 3 MV TandetronTM at IFIN-HH, Romania. *Nuclear Instruments and Methods in Physics Research Section B: Beam Interactions with Materials and Atoms,* 359, pp. 12-19, doi:10.1016/j.nimb.2015.07.011

Carpentier, S.; Pitts, R.A.; Stangeby, P.C.; Elder, J.D.; Kukushkin, A.S.; Lisgo, S.; Fundamenski, W.; Moulton, D. (2011) Modelling of beryllium erosion-redeposition on ITER first wall panels. *Journal of Nuclear Materials*, Vol. 415, https://doi.org/10.1016/j.jnucmat.2010.10.081.

Dinca, P.; Porosnicu, C.; Butoi, B; Jepu, I.; Tiron, V.; Pompilian, O.G.; Burducea, I.; Lungu, C.P.; Velicu, I-L. (2017) Beryllium-tungsten study on mixed layers obtained by m-HiPIMS/DCMS techniques in a deuterium and nitrogen reactive gas mixture, *Surface and Coatings Technology, 321* doi:10.1016/j.surfcoat.2017.04.074.

Dinca, P.; Staicu, C.; Porosnicu, C.; Pompilian, O.G.; Banici, A.-M.; Butoi, B.; Lungu, C.P.; Burducea, I. (2021) Deuterium Retention and Release Behavior from Beryllium Co-Deposited Layers at Distinct Ar/D Ratio. *Coatings, 11*(12), doi: 10.3390/coatings11121443

Dinca, P.; Staicu, C.; Porosnicu, C.; Butoi, B.; Pompilian, O.G.; Banici, A.M.; Baiasu, F.; Burducea, I.; Lungu, C.P. (2022) Deuterium Retention in Mixed Layers with Application in Fusion Technology. *Coatings, 12*(7), 951, doi: 10.3390/coatings12070951

Federici, G.; Andrew, P.; Barabaschi, P.; Brooks, J.; Doerner, R.; Geier, A.; Herrmann, A.; Janeschitz, G.; Krieger, K.; Kukushkin, A.; et al. (2003) Key ITER plasma edge and plasma-material interaction issues. *Journal of Nuclear Materials*, Vol. 313-316, https://doi.org/10.1016/S0022-3115(02)01327-2

Federici, G.; Anderl, R.A.; Andrew, P.; Brooks, J.N.; Causey, R.A.; Coad, J.P.; Cowgill, D.; Doerner, R.P.; Haasz, A.A.; Janeschitz, G.; et al. (1999) In-vessel tritium retention and removal in ITER. *J. Nucl. Mater., 266,* doi:10.1016/S0022-3115(98)00876-9.

Heinola, K.; Ahlgren, T.; Nordlund, K.; Keinonen, J., (2010) Hydrogen interaction with point defects in tungsten, *Physical review. B, Condensed matter*, 82(9):094102, doi: 10.1103/PhysRevB.82.094102.

Johnson, D.F., Carter, E.A., (2010) Hydrogen in tungsten: absorption, diffusion, vacancy trapping, and decohesion, *Journal of Materials Research*, *25*, pp. 315-327, doi: 10.1557/JMR.2010.0036.

Kallenbach, A.; Balden, M; Dux, R.; Eich, T.; Giroud, C.; Huber, A.; Maddison, G.P.; Mayer, M.; McCormick, K.; Neu, R.; Petrie, T.W.; Pütterich, T.; Rapp, J.; Reinke, M.L.; Schmid, K.; Schweinzer, J.; Wolfe, S. (2011) Plasma surface interactions in impurity seeded plasmas. *Journal of Nuclear Materials*, 415(1): S19-S26, doi:10.1016/j.jnucmat.2010.11.105.

Kallenbach, A.; Dux, R.; Fuchs, J.C.; Fischer, R.; Geiger, B.; Giannone, L.; Herrmann, A.; Lunt, T.; Mertens, V.; McDermott, R.; Neu, R.; Pütterich, T.; Rathgeber, S.; Rohde, V.; Schmid, K.; Schweinzer, J.; Treutterer, W. (2010) Divertor power load feedback with nitrogen seeding in

ASDEX Upgrade, *Plasma Physics and Controlled Fusion*, 52, doi:10.1088/0741-3335/52/5/055002.

Krat, S.; Mayer, M.; von Toussaint, U.; Coad, P.; Widdowson, A.; Gasparyan, Y. et al. (2017) Beryllium film deposition in cavity samples in remote areas of the JET divertor during the 2011-2012 ITER-like wall campaign. *Nucl. Mater. Energy*, 12 doi:10.1016/j.nme.2016.12.005.

Krat, S.; Gasparyan, Y.; Vasina, Y.; Davletiyarova, A.; Pisarev, A. (2018) Tungsten-deuterium co-deposition: Experiment and analytical description. *Vacuum*, vol. 149, pp. 23-28, doi:10.1016/j.vacuum.2017.12.004

Krat, S., Gasparyan, Y; Pisarev, A.; Mayer, M.; von Toussaint, U.; Coad, P. et al., (2015) Hydrocarbon film deposition inside cavity samples in remote areas of the JET divertor during the 1999-2001 and 2005-2009 campaigns, *Journal of Nuclear Materials, 463,* https://doi:10.1016/j.jnucmat.2014.10.055.

Malinský, P.; Slepička, P.; Hnatowicz, V.; and Švorčík, V. (2012) Early stages of growth of gold layers sputter deposited on glass and silicon substrates, *Nanoscale Research Letters*, 7(1): 241, doi: 10.1186/1556-276X-7-241

Mayer, M.; Behrisch, R.; Plank, H.; Roth, J.; Dollinger, G.; Frey, C.M. (1996) Codeposition of hydrogen with beryllium, carbon and tungsten, *Journal of Nuclear Materials, 230*, pp. 67-73, doi:10.1016/0022-3115(95)00239-1.

Mayer, M.; Krat, S.; Baron-Wiechec, A.; Gasparyan, Y.; Heinola, K.; Koivuranta, S.; Likonen, J.; Ruset, C.; De Saint-Aubin, G.; Widdowson, A. (2017) Erosion and deposition in the JET divertor during the second ITER-like wall campaign. *Physica Scripta*, Vol. 2017

Mayer, M. (1997) "SIMNRA User's Guide", Tech. Report IPP, 9/113. Rep. IPP 1997

Pacher, G.W. ; Pacher, H.D.; Janeschitz, G.; Kukushkin, A.S.; Kotov, V.; Reiter, D. (2007) Modelling of DEMO core plasma consistent with SOL/divertor simulations for long-pulse scenarios with impurity seeding, *Nuclear Fusion, 47,* doi:10.1088/00295515/47/5/012.

Poon, M.; Haasz, A.A.; Davis, J.W. (2008) Modelling deuterium release during thermal desorption of D+-irradiated tungsten. *Journal of Nuclear Materials*, *374*(3), pp. 390-402, doi:10.1016/j.jnucmat.2007.09.028

Qiao, L.; Zhang, H.W.; Xu, J.; Chai, L.Q.; Hu, M.; Wang, P. (2018) Deuterium retention and release behaviours of tungsten and deuterium co-deposited layers. *Journal of Nuclear Materials*, 502, pp. 247-254, doi:10.1016/j.jnucmat.2018.02.009.

Roth, J.; Tsitrone, E.; Loarer, T.; Philipps, V.; Brezinsek, S.; Loarte, A. et al. (2008) Tritium inventory in ITER plasma-facing materials and tritium removal procedures. *Plasma Phys. Contr. Fusion*, *50*, doi:10.1088/0741-3335/50/10/103001.

Rubel, M.; Philipps, V.; Marot, L.; Petersson, P.; Pospieszczyk, A.; Schweer, B. (2011) Nitrogen and neon retention in plasma-facing materials. *Journal of Nuclear Materials*, Vol. 415.

Schmid, K.; Krieger, K.; Lisgo, S.W.; Meisl, G.; Brezinsek, S. (2015) WALLDYN simulations of global impurity migration in JET and extrapolations to ITER. *Nuclear Fusion*, 55, doi:10.1088/0029-5515/55/5/053015.

Taylor, N.; Alejaldre, C.; Cortes, P. (2013) Progress in the safety and licensing of ITER. *Fusion Sci. Technol.*, 64, doi:10.13182/FST13-A18064.

De Temmerman, G.; Baldwin, M.J.; Doerner, R.P.; Nishijima, D.; Schmid, K. (2008) An empirical scaling for deuterium retention in co-deposited beryllium layers, *Nuclear Fusion, 48,* doi:org/10.1088/0029-5515/48/7/075008.

De Temmerman, G.; Doerner, R.P. (2009) Deuterium retention and release in tungsten co-deposited layers, *Journal of Nuclear Materials, 389,* doi: 10.1016/j.jnucmat.2009.03.028

United Nations Development Programme *Human Development Report 2016: Human Development for Everyone*; 2016;

Wang, P.; Jacob, W.; Gao, L.; Elgeti, S.; Balden, M. (2014) Deuterium retention in tungsten films deposited by magnetron sputtering. *Physica Scripta*, Vol. 2014, T159, DOI: 10.1088/0031-8949/2014/T159/014046.

Wang, P.; Jacob, W.; Elgeti, S. (2015) Deuterium retention in tungsten films after different heat treatments. *Journal of Nuclear Materials, 456,* pp. 192-199, doi:10.1016/j.jnucmat.2014.09.023.

Widdowson, A.; Coad, J.P.; Alves, E.; Baron-Wiechec, A.; Catarino, N.; Corregidor, V.; Heinola, K.; Krat, S.; Makepeace, C.; Matthews, G.F.; et al. (2019) Deposition of impurity metals during campaigns with the JET ITER-like Wall. *Nucl. Mater. Energy*, *19*, doi:10.1016/j.nme.2018.12.02

Zheng, S.; King, D.B.; Garzotti, L.; Surrey, E.; Todd T.N. (2016) Fusion reactor start-up without an external tritium source. *Fusion Engineering and Design, 103,* https://doi.org/10.1016/j.fusengdes.2015.11.034

Zibrov, M.; Ryabtsev, S.; Gasparyan, Y.; Pisarev, A. (2016) Experimental determination of the deuterium binding energy with vacancies in tungsten, *Journal of Nuclear Materials, 477*, pp. 292-297, doi: 10.1016/j.jnucmat.2016.04.052.